Hindawi
Shock and Vibration
Volume 2021, Article ID 8899613, 15 pages
https://doi.org/10.1155/2021/8899613

Research Article

Parameters Optimization and Energy Absorption Evaluation of the Steel Ball Friction Energy Absorber

Bin Gong

China Coal Research Institute, Beijing 100013, China

Correspondence should be addressed to Bin Gong; gongbin9440@163.com

Received 20 August 2020; Revised 19 December 2020; Accepted 13 January 2021; Published 23 January 2021

Academic Editor: Stefano Manzoni

The energy absorber is used to simulate the reaction of a working piece subjected to a vibration stimulus, by which the consistent and repeatable reactions to the tool's vibration inputs could be achieved. According to the proposed coupling simulation model by using commercial software RecurDyn and EDEM, the energy dissipated by the energy absorber and the contact force between the drill rod and the piston are evaluated under different load conditions such as the impact frequency and impact stroke. Moreover, the effects of the ball diameter, ball column height, and diameter on the energy absorption characteristics are also studied. The results show that the impact frequency and stroke influence the energy absorber by changing the impact force; the energy absorption is more obvious under higher impact frequency and long impact stroke. The filling ball diameter influences the energy reflectivity by changing the porosity, which is negatively correlated to the energy reflectivity, and a 6 mm filling ball diameter is suggested. The energy reflectivity is inversely proportional to the ball column height and diameter, and the suggested ball column diameter and height are 160 mm and 600 mm, respectively, with energy reflectivity of 0.045. Even when the increase in impact frequency and stroke will increase the contact force, the dynamic load factor decreases. The contact force and dynamic load factor are inversely proportional to the ball column height, but they are not influenced by the ball diameter and the ball column diameter.

1. Introduction

Rock drilling machines are widely used to drill or break the rock and concrete in many areas, such as mining, railway, hydropower, and transportation engineering construction. Figure 1 illustrates the working principle of an impact rock drilling, the drill rod is connected to the drill tail by a postsleeve, and the drill bit is fixed at the end of the drill rod. When the hammer of the rock drilling machine starts to reciprocate under the action of gas or hydraulic pressure, it will impact the drill tail repeatedly, and the impact stress wave propagates from the drill rod to the drill bit and rock and breaks the rock.

To improve the performance and efficiency of the rock drilling machine, predecessors have done a lot of related research, such as the percussive process [1–5], rock breaking mechanism [6–8], stress wave propagation [9], and energy transfer efficiency [5, 10–13]. However, a reliable and effective test method is also required for performance evaluation when developing or optimizing the rock drilling machine. Clarke et al. fixed an accelerometer into the mounting block welded on the chisel to measure the vibration emitted by percussive tools, but problems such as the fracturing of the weld holding the block to the chisel, and the unscrewing of the stud holding the accelerometer to the block were encountered during the test [14]. Because measuring vibration on a chisel is extremely difficult, Bitsch et al. fixed the accelerometers on the handle instead of the chisel and developed a test code for the measurement of vibration from percussive tools under laboratory conditions [15].

As it is usually very difficult to obtain highly repeatable test data at real workplaces in the field due to the difficulties of controlling all of the variables associated with the complex working environments, the International Organization for Standardization (ISO) developed the methods for performance tests of rotary and percussive pneumatic tools [16] and measuring the vibrations at the handle for hand-held portable power tools [17]. In these methods, an energy absorber is used as a key device to simulate the reaction of a

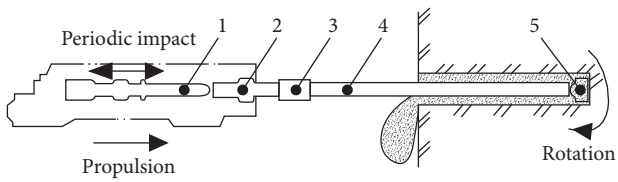

Figure 1: Working principle of an impact rock drilling (1: hammer of the rock drill, 2: drill tail, 3: post sleeve, 4: drill rod, and 5: drill bit).

working piece subjected to a vibration stimulus, by which the consistent and repeatable reactions to the tool's vibration inputs could be achieved, as shown in Figure 2. Moreover, the energy absorber could also eliminate excess vibration of the drill rod and avoid the interference of the reflected waves. As there is no uniform regulation on the structure and type of energy absorbers, different energy absorbers were used in studies. In the impact energy test system developed by Park et al., a target base was constructed with accumulating vibration-isolating materials like sands, broken stones, trees, and rubbers after 5 m depth foundation work to absorb shock and vibration at blowing [18]. Seo et al. used a 110 mm steel plate made of SS400 to bear the impact of the drifter rod when evaluating the percussion performance of rock drill drifter [19, 20].

Even though research has been carried out to evaluate the performance of the rock drill using the stress wave method and energy absorber, the comments on the energy absorber are rare. Bitsch et al. used six different energy absorption methods, which are the hydraulic base, the steel shot, the actual breaking of concrete, the AFNOR concrete block, and the pointed chisel embedded in concrete, to simulate the actual working condition in the handle vibration measurement of percussive tools, the results showed that the different methods tested were all valid and comparable to those obtained when real concrete was broken. Moreover, they proposed that, for the steel shot energy absorption method, the box diameter should be at least 500 mm, and the depth of the shot should be 300 mm [15]. According to international standard ISO 8662-2, the energy absorber device should avoid energy reflection, and the reflected energy should not exceed 20% of the incident energy [17], but it is not mentioned in the comments of Bitsch et al. [15]. Zheng et al. presented the working mechanism of an energy absorber by the friction of steel balls and obtained the reflective properties of the steel balls, the optimum cross-section ratio of the absorber to the drill rod, the energy absorption coefficient, and the reasonable ball column length by using the wave principle [21]. Dong et al. investigated the vibration characteristics of the chipping hammers operating on an energy absorber to evaluate the test procedures mentioned in ISO 8662-2 [22]; in this study, the energy absorber was similar to the absorber mentioned by Zheng et al. [21], which was composed of a steel tube filled with hardened steel balls and firmly mounted on a rigid steel base that is secured to a concrete block. They found that the feed forces and the vibration emission associated with the energy absorber are affected by the feed force, the energy

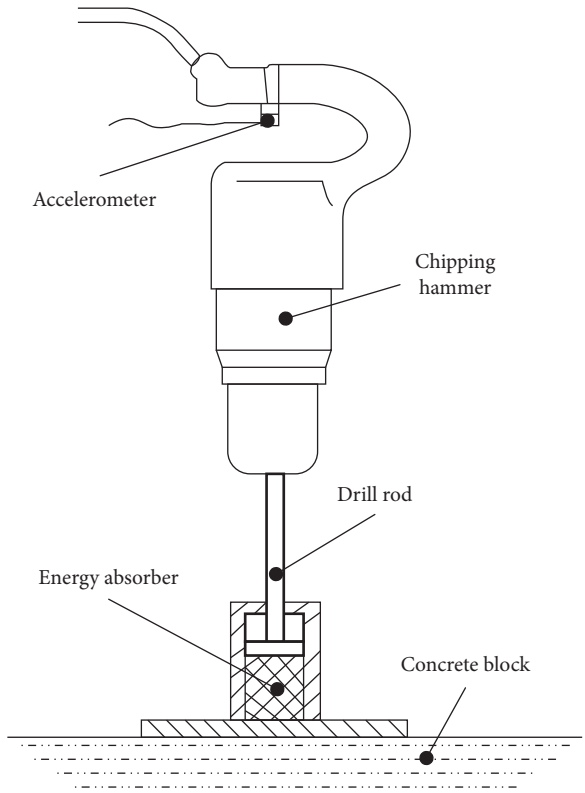

Figure 2: The measurement setup for the ISO standardized chipping hammer test [17].

absorber at the higher feed force does not provide stable feedback, and the vibration emission is not reasonably repeatable.

As the energy absorber provides very consistent working conditions for different subjects, requires little maintenance, and can be used repeatedly for the experiment, it is essential to understand the characteristics of the energy absorber and optimize its structure to satisfy the demand that the reflected energy should not exceed 20% of the incident energy [17]. This study investigates the energy absorption characters of the steel ball friction energy absorber and provides the relationship between the energy absorption efficiency and the structural parameters of the energy absorber.

2. Energy Absorber Model in RecurDyn

2.1. Geometry Model and Material Model. According to the structural schematic diagram of the steel ball friction energy absorber [22], the simplified geometry of the energy absorber is shown in Figure 3(a), it is composed of a cylinder, a piston, steel balls, and a drill rod. The geometry model without steel balls was created in RecurDyn according to the parameters listed in Table 1, a coupled model will be created in EDEM to generate the steel balls and simulate the collision behavior of the balls. The coordinate origin of the model locates at the center of the bottom surface of the piston; the gravity direction is along the −z-axis. The cylinder and the piston are assumed as a rigid body, and the drill rod is

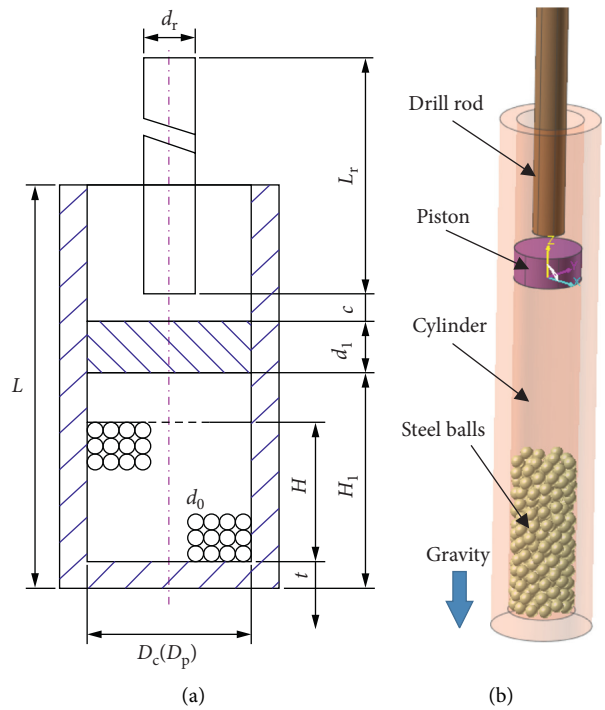

Figure 3: Steel ball friction energy absorber. (a) Geometric dimension. (b) Model in RecurDyn.

Table 1: Geometric dimension of the energy absorber.

Part name	Parameters	Values (mm)
Cylinder	Inner diameter, D_c	40
	Wall thickness, t	10
	Length, L	320
Piston	Piston diameter, D_p	40
	Piston thickness, d_1	19
Ball column	Column height, H	100
	Ball diameter, d_0	8
Drill rod	Diameter, d_r	19
	Length, L_r	3000
Assembly size	Clearance, c	10
	Piston position, H_1	150

modeled as a flexible body of steel with elastic modulus $E = 210$ GPa and Poisson's ratio $\upsilon = 0.3$.

2.2. Joints and Contacts. It is assumed that the cylinder of the energy absorber is fixed to a concrete base, the drill rod moves reciprocally under the hit of a rock drill machine hammer, and, also, the piston moves reciprocally under the hit of the drill rod. So, the drill rod and the piston are restricted by a cylindrical joint, by which they could only move along the z-axis and rotate around the z-axis [23]. In an actual working condition, the cooling water will pass through the clearance between the cylinder and piston, so the static friction coefficient and dynamic friction coefficient are 0.08 and 0.05, respectively, between greasy steels.

The contacts are introduced between the drill rod and the piston, the piston, and the cylinder. The simulation parameters used to define the contact relationship are shown in Table 2.

2.3. Load Condition. As shown in Figure 1, the hammer of the rock drill impacts the drill rod continuously so that the drill rod obtains kinetic energy. Therefore, the impact force between the hammer and the drill rod could be applied to the model as a load condition. According to the impulse theorem,

$$F = \frac{m_r \Delta v_r}{t}, \tag{1}$$

where F denotes the impact force between the hammer and the drill rod, N; m_r is the mass of the drill rod, kg; t is the impact duration between the hammer and the drill rod, s; and Δv_r is the velocity change of the drill rod before and after impact, m·s^{-1}.

For an elastic collision, when the hammer of a rock drill hit the drill rod, according to the law of conservation of momentum and the law of conservation of mechanical energy, we can get

$$\begin{aligned} m_h v_h + m_r v_r &= m_h v_h' + m_r v_r', \\ \frac{1}{2} m_h v_h^2 + \frac{1}{2} m_r v_r^2 &= \frac{1}{2} m_h v_h'^2 + \frac{1}{2} m_r v_r'^2, \end{aligned} \tag{2}$$

where m_h denotes the mass of hammer, kg; v_h and v_r are the velocity of the hammer and the drill rod before impact, m·s^{-1}; and v_h' and v_r' are the velocity of the hammer and the drill rod after impact, m·s^{-1}.

According to equation (2),

Table 2: Parameters to define the contact relationship.

Parameters	Values
Stiffness coefficient, k (N·mm^{-1})	10 000
Damping coefficient, ζ (N·s·mm^{-1})	50
Static friction coefficient, f_s	0.08
Dynamic friction coefficient, f_d	0.05
Stiffness exponent, n	1.5
Static threshold velocity, v_s (mm·s^{-1})	0.1
Dynamic threshold velocity, v_d (mm·s^{-1})	10

$$v'_{\mathrm{hr}} = -v_{\mathrm{hr}}, \tag{3}$$

where v_{hr} and v'_{hr} are the relative velocity between the hammer and the drill rod before and after the impact:

$$\begin{aligned} v_{\mathrm{hr}} &= v_h - v_r, \\ v'_{\mathrm{hr}} &= v'_h - v'_r. \end{aligned} \tag{4}$$

If the collision is inelastic, the relative velocity will decrease due to the kinetic energy dissipating, by introducing the coefficient of restitution e:

$$e = -\frac{v'_{\mathrm{hr}}}{v_{\mathrm{hr}}}. \tag{5}$$

It is obvious that $0 \le e \le 1$; the collision is elastic when $e = 1$; and the two parts will stick together with $e = 0$. If $0 \le e < 1$, the collision is inelastic, and the velocities of the hammer and drill rod after the impact could be achieved as

$$\begin{aligned} v'_h &= v_h - \frac{m^*}{m_{\mathrm{h}}}(1+e)v_{\mathrm{hr}}, \\ v'_r &= v_r + \frac{m^*}{m_{\mathrm{r}}}(1+e)v_{\mathrm{hr}}, \end{aligned} \tag{6}$$

where m^* is the equivalent mass:

$$m^* = \frac{m_h m_r}{m_h + m_r}. \tag{7}$$

The hammer of the rock drill machine reciprocates periodically under the action of gas; assuming it is uniform motion, the velocity of the hammer before impact is

$$v_{\mathrm{h}} = 2L_{\mathrm{s}} f, \tag{8}$$

where L_{s} is the stock of the hammer, m, and f is the reciprocating frequency of the hammer, Hz.

Generally, the hammer reciprocates with a frequency of 30–40 Hz and a stroke of 50–80 mm. With a density $\rho = 7800\,\mathrm{kg{\cdot}m^3}$, the mass of the drill rod is $m_{\mathrm{r}} = 8.34$ kg. Assuming the initial velocity of the drill rod is 0, the impact duration $\Delta t = 0.001$ s and the coefficient of restitution $e = 0.5$ [24–26]. The impact forces bear by the drill rod are calculated under different load conditions, as shown in Table 3.

3. Energy Absorber Model in EDEM

3.1. Geometry Model and Material Model. The model built in EDEM is to generate the steel balls and simulate the collision and friction process among steel balls. The geometry is created by importing the geometric model from RecurDyn, as shown in Figure 4. All materials in EDEM are steel with density $\rho = 7800\,\mathrm{kg{\cdot}m^3}$, elastic modulus $E = 210$ GPa, and Poisson's ratio $\upsilon = 0.3$. The Hertz–Mindlin (no-slip) model and standard rolling friction model [27] are adopted to describe the contact among the cylinder, the piston, and the steel balls. The static friction coefficient f_{s}, the rolling friction coefficient f_{r}, and the coefficient of restitution e are adopted as 0.08, 0.01, and 0.5, respectively.

3.2. Particle Factory. The steel balls are generated in a particle factory, which has the same geometry size related to the ball column. Clearance should be left between the generated balls and the energy absorber bounder to avoid overlap, so the diameter and the height of the particle factory are $(D_{\mathrm{c}} - d_0)/2$ and $H - d_0$, respectively.

The total steel balls generated are determined by the height of the ball column, the inner diameter of the cylinder, and the radius of the balls. The filling ball numbers are different with different stack ways, such as simple cubic (SC), body-centered cubic (BCC), face-centered cubic (FCC), or hexagonal close-packed (HCP). If the balls stack as SC, the arrange of balls is similar to the squares on a single-layer plane as shown in Figure 5, and the ball number on a single plane could be calculated as

$$n_L = 4\sum_{i=1}^{n_0}\left\lfloor \frac{\sqrt{(D_c/2)^2 - (id_0)^2}}{d_0} \right\rfloor, \tag{9}$$

where n_{L} is the ball number on a single plane; $\lfloor\ \rfloor$ denotes round down; n_0 is the stack layers along the radius direction:

$$n_0 = \left\lfloor \frac{D_c/2}{d_0} \right\rfloor. \tag{10}$$

Thus, the total balls filled by SC in the ball column with height H could be calculated approximately as

$$n_{\mathrm{sc}} = n_{\mathrm{L}} \left\lceil \frac{H}{d_0} \right\rceil, \tag{11}$$

where n_{sc} is the ball numbers filled by SC.

According to the crystallographic theory, the packing factors for SC, BCC, FCC, and HCP are 0.524, 0.68, 0.74, and 0.74, respectively; thus, the ball numbers filled with other manners are

$$\begin{aligned} n_{\mathrm{bcc}} &= \frac{0.68}{0.524} n_{\mathrm{sc}} \approx \lceil 1.30 n_{\mathrm{sc}} \rceil, \\ n_{\mathrm{fcc}} &= n_{\mathrm{hcp}} = \frac{0.74}{0.524} n_{sc} \approx \lceil 1.41 n_{\mathrm{sc}} \rceil, \end{aligned} \tag{12}$$

where n_{bcc}, n_{fcc}, and n_{hcp} are the ball numbers filled with BCC, FCC, and HCP, respectively.

The ball generation velocity is

$$v_{\mathrm{gen}} = \frac{n}{t_{\mathrm{gen}}}, \tag{13}$$

Table 3: Impact force under different load conditions.

Hammer			Drill rod
Impact frequency f(HZ)	Impact stock L_s (mm)	Mass m_1 (kg)	Impact force F(N)
30	50	1.95	1348
30	50	2.15	1577
30	80	1.95	2157
30	80	2.15	2523
40	50	1.95	1798
40	50	2.15	2103
40	80	1.95	2876
40	80	2.15	3364

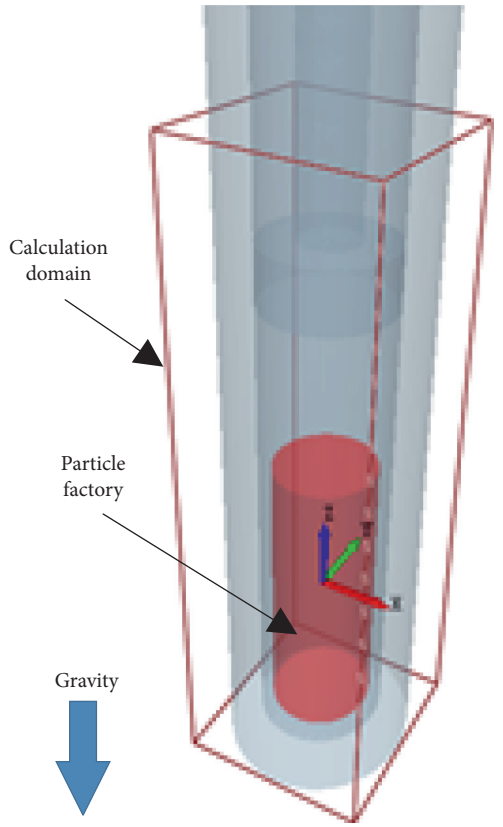

Figure 4: Simulation model in EDEM.

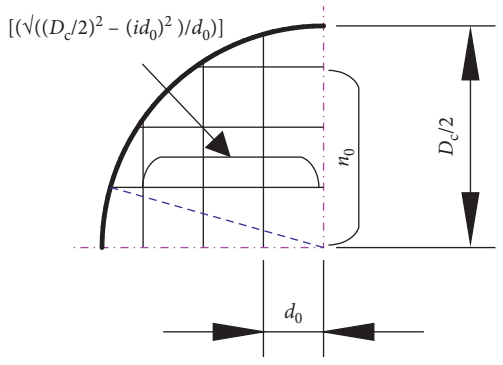

Figure 5: Schematic diagram of single-layer ball filling (within 1/4 of a circle).

where v_{gen} is the ball generation velocity s^{-1} and n is the total ball number that should be generated in period t_{gen}.

3.3. Calculation Domain and Environment. The calculation domain is built containing the internal area of the cylinder as shown in Figure 4, the gravity g is along the $-z$-axis, and the grid size equals $2r_0$. The solver settings are different in different simulations due to the ball radius, density, and so forth, and they are not discussed here.

4. Impact Process and Evaluation Method of the Energy Absorber

4.1. Motion Process of the Drill Rod under Periodic Pulse Force. Under the periodic impact with $f = 30$ Hz, $L_s = 50$ mm, the motion of the drill rod is periodic. To analyze the motion process of the drill rod in detail, the parameters such as rod position, velocity, acceleration, and the contact force between the drill rod and the piston are shown in Figures 6 and 7 between 0.4 s and 0.6 s. The motion of the drill rod is divided into four stages in a cycle.

(1) The hammer impact stage: at time A, the hammer starts to impact the rod, the rod is accelerated along the $-z$-axis, the velocity of the rod decreases quickly from 200 mm·s^{-1} at time A to 0 at time B, and the rod has the highest position at this moment. The rod acquires the largest acceleration along the z-direction at time C, and the largest velocity along the $-z$-direction appears a little later at moment D when the acceleration reduces to 0. However, the acceleration and velocity of the rod keep oscillating and eventually stabilize; this is because the drill rod is restricted by a cylindrical joint with friction, and it constitutes a second-order underdamped system. Under an impact load, the acceleration of the rod will resume to the initial value at time E shown in Figure 6. However, the velocity of the rod affected by the acceleration will not resume, but a stable value is achieved at moment E.

(2) The motion under gravity: when the impact load releases and the acceleration achieves the stable value at moment E, the forces acting on the rod are the gravity and the sliding friction and the acceleration of the rod is close to the acceleration of the gravity until time F. Between times E and F, the acceleration of the rod is approximately constant and the velocity of the rod increases linearly along the $-z$-direction.

(3) Contact and rebound: at time F, the rod contacts with the piston, and the piston together with the rod starts receiving the reaction force of the ball column along the $+z$-direction. As the piston moves along the $-z$-direction continuously, the contact force between the rod and the piston increases, along with the acceleration changing to the $+z$-direction and keeps increasing; the velocity of the rod starts to change from about −650 mm·s^{-1} to 0 at time G. At this moment, the rod can get the lowest position, and the contact forces between the rod and the piston are the largest. After time G, the piston and the rod start to move along the $+z$-direction, with the contact force decreasing accompanied by the decrease in acceleration along the $+z$-direction. However, the velocity of the rod keeps increasing because an acceleration along +z exists.

(4) Disengagement of the piston and the ball column: at time H, the contact force between the rod and the piston reduces to 0, which means that the piston and the ball column have been out of contact. The piston and rod continue to move along the $+z$-direction under the +z velocity; however, the velocity of the rod starts to decrease under the gravity until the next cycle starts at moment J.

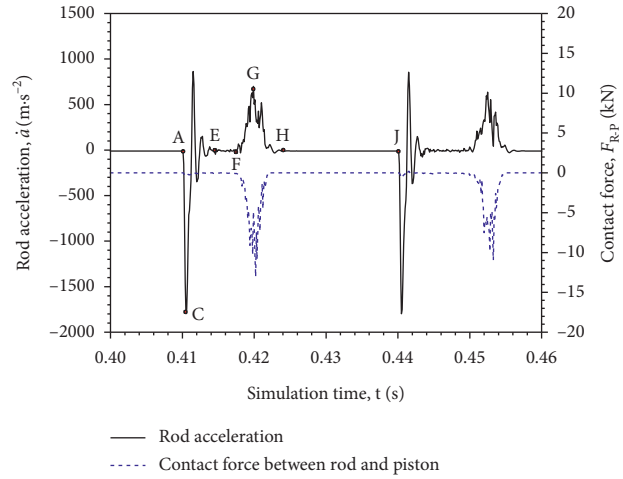

Figure 6: Rod acceleration and contact force between the drill rod and piston.

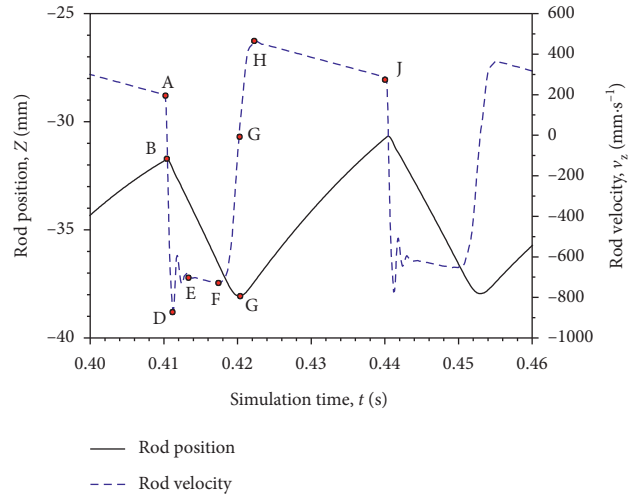

Figure 7: Position and velocity of the drill rod.

4.2. Energy Absorption Evaluation Methods of the Energy Absorber. According to the motion process of the drill rod under periodic pulse force, the drill rod is the energy transfer

medium between the rock drill and the energy absorber. The drill rod obtains kinetic energy after the impact of the hammer. When the drill rod impacts the piston, parts of the rod kinetic energy are stored by the ball column as elastic energy; then, some of the elastic energy stored will be reflected in the drill rod as kinetic energy, and the others will be dissipated by the energy absorber. Thus, the energy absorbed by the energy absorber is

$$\mathrm{E}_{\mathrm{absorb}} = \mathrm{E}_{\mathrm{impact}} - \mathrm{E}_{\mathrm{rebound}}, \tag{14}$$

where $\mathrm{E}_{\mathrm{absorb}}$ is the energy dissipated by the energy absorber; $\mathrm{E}_{\mathrm{impact}}$ is the kinetic energy of the drill rod after the impact of the hammer; and $\mathrm{E}_{\mathrm{rebound}}$ is the kinetic energy of the drill rod after the rebound:

$$\begin{aligned} E_{\mathrm{impact}} &= \frac{1}{2} m_{\mathrm{r}} v_{\mathrm{impact}}^2, \\ E_{\mathrm{rebound}} &= \frac{1}{2} m_{\mathrm{r}} v_{\mathrm{rebound}}^2, \end{aligned} \tag{15}$$

where v_{impact} and v_{rebound} are the initial velocity of drill rod after the impact and the rebound, respectively.

The energy reflectivity γ and energy dissipation rate η could be defined as

$$\begin{aligned} \gamma &= \frac{E_{\mathrm{rebound}}}{E_{\mathrm{impact}}} = \frac{v_{\mathrm{rebound}}^2}{v_{\mathrm{rebound}}^2}, \\ \eta &= \frac{E_{\mathrm{absorb}}}{E_{\mathrm{impact}}} = 1 - \frac{E_{\mathrm{rebound}}}{E_{\mathrm{impact}}} = 1 - \gamma. \end{aligned} \tag{16}$$

The drill rod has different impact velocity v_{impact} and rebound velocity v_{rebound} in every cycle according to Figure 7; thus, two methods are proposed to calculate the average energy reflectivity:

$$\begin{aligned} \overline{\gamma} &= \frac{\overline{E}_{\mathrm{rebound}}}{\overline{E}_{\mathrm{impact}}} = \frac{\overline{v}_{\mathrm{rebound}}^2}{\overline{v}_{\mathrm{impact}}^2}, \\ \overline{\gamma}' &= \frac{1}{k} \sum_{i=1}^{k} \gamma_i = \frac{1}{k} \sum_{i=1}^{k} \frac{v_{\mathrm{rebound}}^2}{v_{\mathrm{impact}}^2}. \end{aligned} \tag{17}$$

In equation (17), the energy reflectivity $\overline{\gamma}$ is calculated by the average velocity of v_{impact} and v_{rebound} during the observation, while the energy reflectivity $\overline{\gamma}'$ in equation (17) is the average energy reflectivity of each cycle during the observation. The energy dissipation rate also has similar calculation methods:

$$\begin{aligned} \overline{\eta} &= 1 - \overline{\gamma}, \\ \overline{\eta}' &= 1 - \overline{\gamma}'. \end{aligned} \tag{18}$$

5. Influence of Energy Absorber Structure Parameters on Energy Absorption Effect

5.1. Effects of Impact Frequency and Stroke on the Energy Absorption Effect. The impact frequency and stroke of the hammer eventually change to the frequency and magnitude of the impact force, which acts on the drill rod. The impact forces under different load conditions are listed in Table 3; four impact forces of 1348 N, 1798 N, 2523 N, and 3364 N are selected to evaluate the effects of impact frequency and stroke on energy absorption.

5.1.1. The Maximum Impact Velocity and Rebound Velocity of the Drill Rod. Figure 8 shows the maximum impact velocity and maximum rebound velocity of the drill rod under different impact conditions. It can be seen that when the impact stroke increases from 50 mm to 80 mm, the maximum impact velocity and maximum rebound velocity of the drill rod increase with an impact frequency of either 30 Hz or 40 Hz. The maximum impact velocity and maximum rebound velocity of the drill rod also increase when the impact frequency increases from 30 Hz to 40 Hz when keeping the stroke L_{s} unchanged. The increases in impact frequency or stroke will both improve the maximum impact velocity and the rebound velocity of the drill rod. This is because the impact frequency and stroke are related to the initial velocity of the hammer according to equation (8) and eventually change to the periodic pulse force applying to the simulation model by equations (1) and (6). The impact forces converted by different impact frequencies and strokes are shown in Figure 8, and a positive correlation between the impact force and the velocity of the drill rod could be found. Moreover, the standard deviation of the drill rod velocity increases with the increasing impact frequency and stroke, which denotes the increased energy fluctuation and unstable working status with high frequency and long stroke.

5.1.2. Energy Reflectivity. The energy reflectivity of the energy absorber shown in Figure 9 is calculated by the two methods of equation (17); the difference between $\overline{\gamma}$ and $\overline{\gamma}'$ is very small, which denotes the two methods are both effective. With the increasing impact frequency and stroke, the energy reflectivity decreases from 0.289 to 0.232. The results denote that the energy absorption effect is more obvious under a larger load. However, the smallest energy reflectivity is 0.232, which is higher than the allowable value of 0.2 in the standard. The energy absorber with a 100 mm ball column and 8 mm diameter balls does not meet the requirements.

5.1.3. The Contact Force between the Drill Rod and the Piston. The contact force between the drill rod and the piston reaches the maximum value when the ball column is compressed to the shortest height; the average contact forces at different impact conditions are shown in Figure 10. The contact forces in Figure 10 are obtained after the low-pass filtering with a second-order Butterworth filter, and the cutoff frequencies of the filter are 100 Hz and 200 Hz, respectively. It is found that the contact force increases with the increase in impact frequency and stroke, and the increased standard deviation denotes a higher fluctuant contact force at a higher impact frequency and long impact stroke. Because part of the fluctuating force between 100 Hz and 200 Hz is filtered by the filter, a higher contact force is

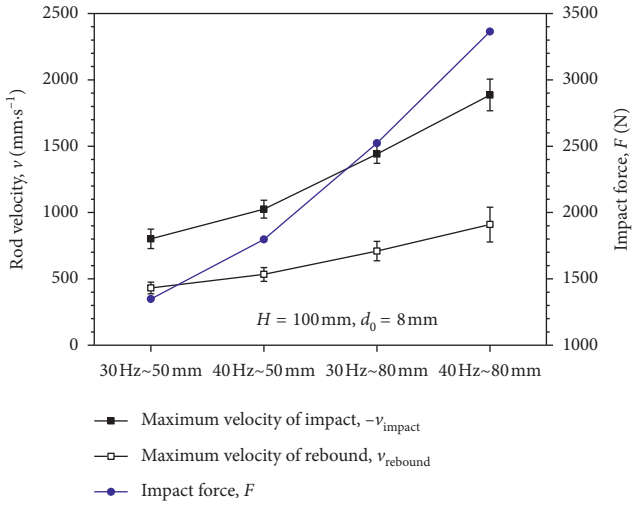

FIGURE 8: Impact velocity and rebound velocity of the drill rod under different impact parameters.

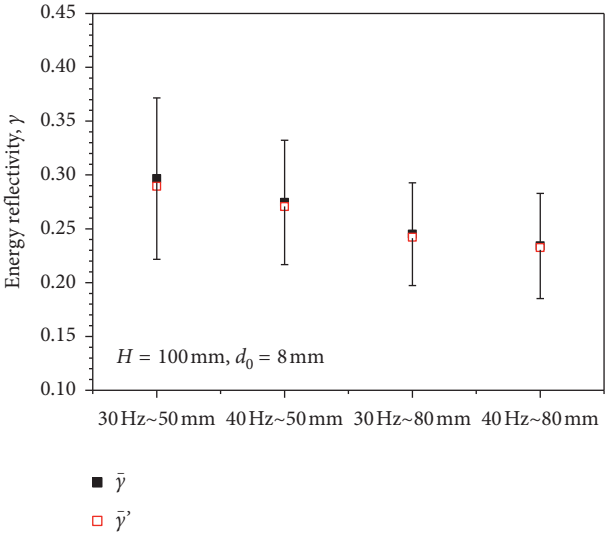

FIGURE 9: Energy reflectivity under different impact parameters.

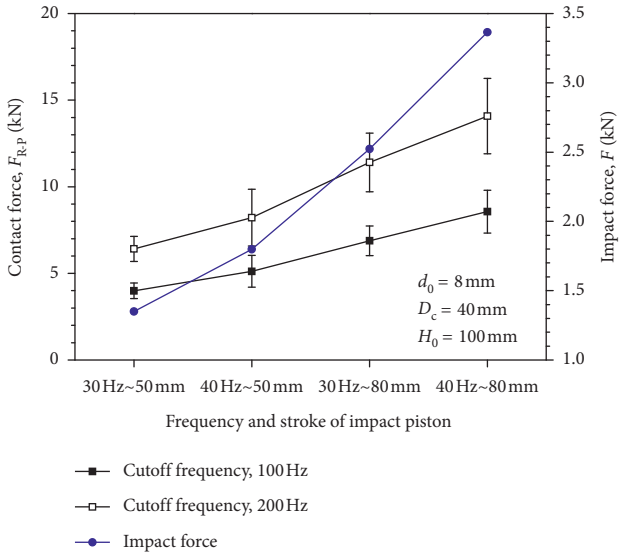

FIGURE 10: Contact force under different impact parameters.

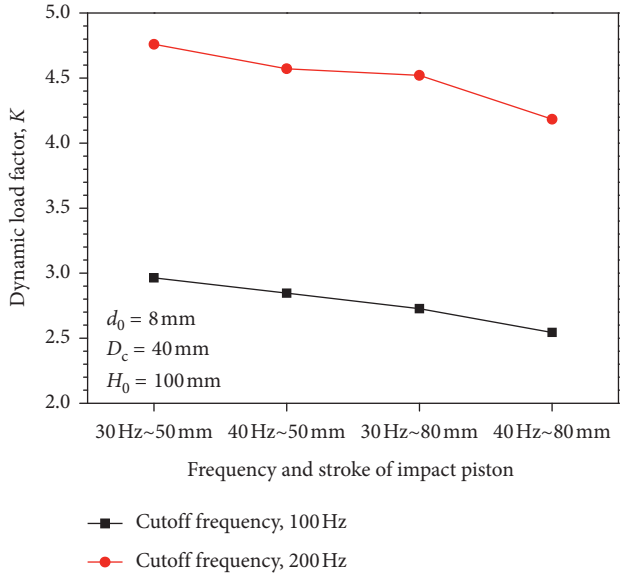

FIGURE 11: Dynamic load factor under different impact parameters.

obtained with the cutoff frequency of the filter equal to 200 Hz.

Whether the contact force filtered by the filter of 100 Hz or 200 Hz, its value is higher than the impact force applied; this is because the contact force between the drill and the piston belongs to dynamic load, which is higher than the applied static load. Define dynamic factor as

$$K = \frac{F_{R-P}}{F}, \tag{19}$$

where $F_{R\text{-}P}$ is the maximum contact force between the drill rod and the piston, kN, and F is the periodic impact force applied to the drill rod, kN.

Figure 11 demonstrates the dynamic load factor under different impact frequencies and strokes; with an increased impact frequency and stroke, the dynamic load factor decreases from 2.96 to 2.54 or from 4.76 to 4.18 under a different filter. The dynamic factor reduction rate is 14% or 12%, which also denotes more obvious energy absorption efficiency under a higher load.

5.2. Effects of Ball Diameter on the Energy Absorption. For a steel ball friction energy absorber, the ball column is the core part, which is designed to absorb the impact energy. The geometry size of the ball column contains height, column diameter, and steel ball diameter. In this section, the steel ball with diameters of 4 mm–8 mm is adopted to study the effects of ball diameter on energy absorption. Even though the impact frequency and stroke influence the energy absorption effect, they are external input parameters and cannot determine the inherent characteristics of energy absorption. However, the stable working status of the energy absorber is beneficial to the postprocessing of the data, so a

lower impact frequency of 30 Hz and a short impact stroke of 50 mm are selected as load condition; the equivalent impulse force is 1348 N.

5.2.1. The Maximum Impact Velocity and Rebound Velocity of the Drill Rod. Figure 12 shows the maximum impact velocity and maximum rebound velocity of the drill rod with different filling ball diameters, the maximum impact velocities, and rebound velocities change in the ranges of 800 mm·s^{-1}~840 mm·s^{-1} and 428–442 mm·s^{-1}, respectively. The values have no obvious increasing or decreasing trend with a decreased ball diameter, which indicates the ball diameter has a few effects on the impact velocity and the rebound velocity of the drill rod. The rod velocity has the smallest standard deviation with the ball diameter equal to 6 mm, indicating a more stable working status of this condition.

5.2.2. Energy Reflectivity. The energy reflectivity of the energy absorber shown in Figure 13 is with different filling ball diameters, which also show that there is no difference between the two energy reflectivity calculation methods. When the ball diameter decreases from 8 mm to 7 mm, the energy reflectivity decreases from 0.296 to 0.282. If the ball diameter keeps decreasing from 7 mm to 4 mm, the energy reflectivity gradually increases to 0.306. Although the changing trend is very weak, an inverted parabolic relationship could be found between the energy reflectivity and ball diameter, and the smallest energy reflectivity appears at the ball diameter equal to 7 mm. The result could be related to the filling ball number concerning the porosity. Define the filling ratio and porosity of the ball column as

$$\phi = \frac{nV_b}{V_c} = \frac{2}{3}\frac{nd_0^2}{H'D_c^2}, \qquad \lambda = 1 - \phi, \tag{20}$$

where ϕ is the filling ratio of the ball column, which denotes the substantial proportion of entities in the ball column. On the contrary, λ is the porosity of the ball column, which denotes the volume occupancy ratio of the pores in the ball column; V_b and V_c are the volumes of a steel ball and the ball column, respectively; n is the filled ball numbers in the ball column; and H' is the height of the ball column under the maximum compression.

Table 4 lists the filling ratio and porosity of the ball column with different ball diameters; it is found that the porosity has the highest value of 0.434 with the ball diameter equal to 7 mm, which corresponds to the lowest energy reflectivity of 0.267.

When the ball diameter decreases from 7 mm to 4 mm, the porosity of the ball column decreases to 0.299 gradually, along with an increasing energy reflectivity from 0.267 to 0.302. When the ball diameter increases from 7 mm to 8 mm, the porosity of the ball column decreases to 0.379, along with an increased energy reflectivity. It is found that whether the diameter and energy emissivity are positively or negatively correlated, the energy reflectivity is negatively correlated with the porosity. According to the limit value of porosity and energy reflectivity in Table 4, it is calculated that the energy reflectivity will reduce to 0.259 per unit change of porosity.

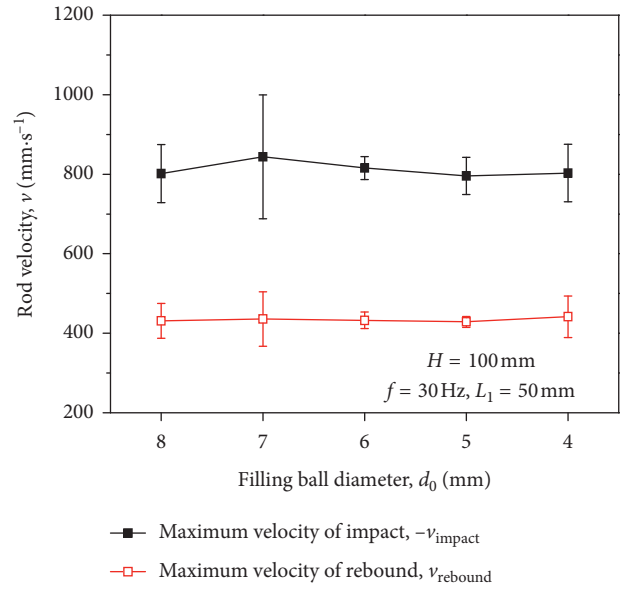

Figure 12: Impact velocity and rebound velocity of the drill with a different filling ball diameter.

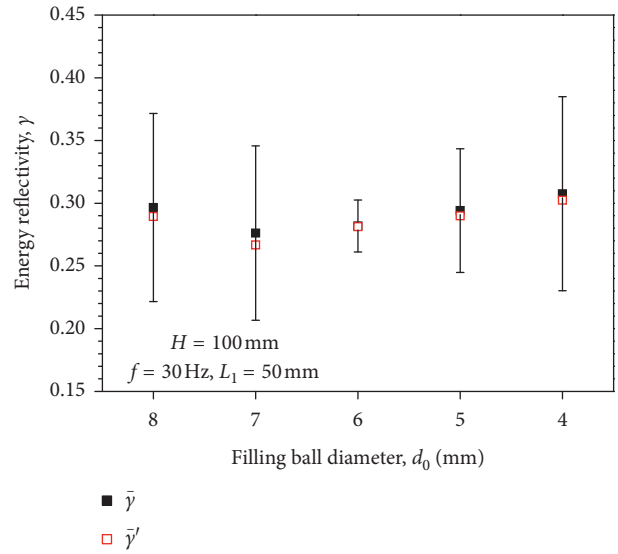

Figure 13: Energy reflectivity under different filling ball diameters.

When the ball diameter changes from 8 mm to 3 mm, the smallest energy reflectivity is 0.267, which is higher than the allowable value of 0.2 in the standard; thus, the other parameters should be considered to further optimize the structure of the energy absorber.

5.2.3. The Contact Force between the Drill Rod and the Piston. The average contact forces and standard deviation with different filling ball diameters are shown in Figure 14; the

Table 4: Filling ratio and porosity of the ball column with different ball diameters.

Ball diameter, d_0 (mm)	Filled ball number, n	Compressed column height, H' (mm)	Filling ratio, ϕ	Porosity, λ	Energy reflectivity, γ
8	269	92.42	0.621	0.379	0.289
7	350	88.33	0.566	0.434	0.267
6	580	90.85	0.575	0.425	0.281
5	1249	94.29	0.690	0.310	0.290
4	2482	94.43	0.701	0.299	0.302

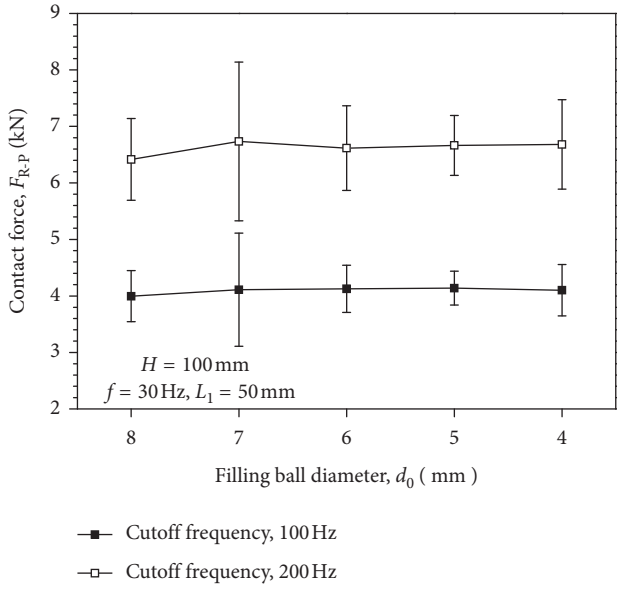

Figure 14: Contact force under different filling ball diameters.

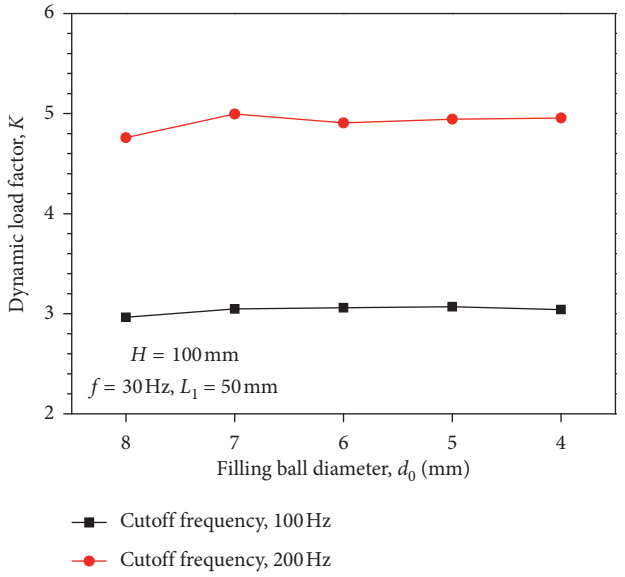

Figure 15: Dynamic load factor under different filling ball diameters.

contact force has no significant change when the ball diameter changes. The standard deviation of the contact force is also the same, besides the ball diameter equal to 7 mm, at which the contact force has a bigger fluctuation. The average contact forces filtered by the filter with the cutoff frequency of 100 Hz and 200 Hz are 4.09 kN and 6.62 kN, respectively. The dynamic load factors shown in Figure 15 are also not related to the filling ball diameter, and the average dynamic load factors are 3.04 and 4.91 with different filters.

5.3. Effects of Ball Column Height on the Energy Absorption. To evaluate the effects of ball column height on the energy absorption, the ball column heights in the range of 100 mm to 180 mm are examined. The filling ball diameter is selected as 6 mm due to the relatively small energy reflectivity and standard deviation, and the equivalent impulse force of 1348 N is adopted.

5.3.1. The Maximum Impact Velocity and Rebound Velocity of the Drill Rod. Figure 16 shows the maximum impact velocity and maximum rebound velocity of the drill rod with ball column height; with an increasing ball column height, the maximum impact velocity increases from 815 mm·s^{-1} to 842 mm·s^{-1} gradually, and the maximum rebound velocity decreases from 432 mm·s^{-1} to 391 mm·s^{-1} on the contrary. The velocities with different ball columns all have a small

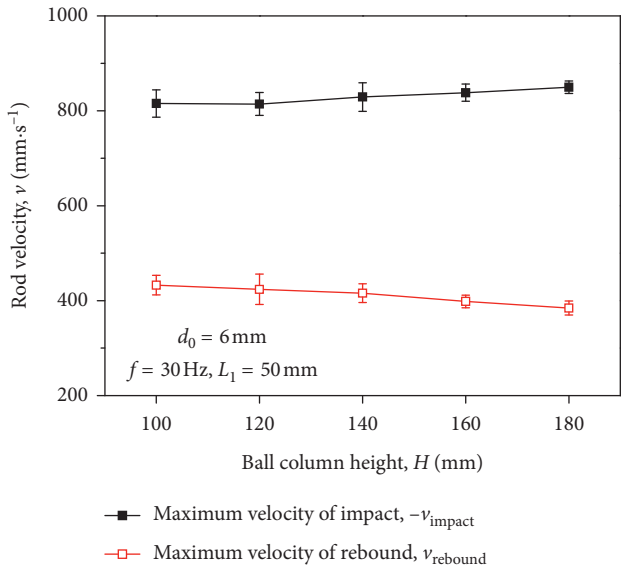

Figure 16: Impact velocity and rebound velocity of the drill with different ball column heights.

standard deviation, and the deviation has a decreasing trend with the increasing column, which indicates that the motion of the drill is stable with the increase in the ball column.

5.3.2. Energy Reflectivity. The energy reflectivity of the energy absorber with different ball column heights is shown in Figure 17, the energy reflectivity calculated by the two methods overlaps with each other except for a minor difference of 0.015 when the ball column height equals 120 mm. When the ball column increases from 100 mm to 180 mm, the energy reflectivity decreases linearly from 0.281 to 0.215, with a reduction of 21%. As listed in Table 5, the porosities of the ball column with different ball column heights have no obvious difference, which indicates that the apparent reduction of energy reflectivity is benefitted from the ball column height. According to the limit value of the porosity and the ball column height in Table 5, it is calculated that the energy reflectivity will reduce by about 0.09 with a 100 mm ball column height increase. However, the smallest energy reflectivity is 0.215, which is still a bit higher than the allowable value of 0.2 in the standard; thus, the other parameters should be considered to further optimize the structure of the energy absorber.

5.3.3. The Contact Force between the Drill Rod and the Piston. The average contact forces and dynamic load factors with different filling ball diameters are shown in Figures 18 and 19, respectively, both of them decrease with the increasing ball column. When the ball column height increases from 100 mm to 180 mm, both the contact force and dynamic factor have a reduction of 5.8% or 9.7% under different filters. The results indicate that the increase in the ball column height is beneficial to reducing the contact force. However, it could be found that the contact force reduction effect introduced by the increasing ball column decreases with the increasing ball column height.

5.4. Effects of Ball Column Diameter on the Energy Absorption. The optimal parameters of the energy absorber that have been achieved, which are the ball diameter of 6 mm and ball column height of 180 mm, are selected to study the effects of ball column diameter on the energy absorption. The equivalent impulse force of 1348 N is still adopted.

5.4.1. The Maximum Impact Velocity and Rebound Velocity of the Drill Rod. Figure 20 shows the maximum impact velocity and maximum rebound velocity of the drill rod with ball column diameter and the maximum impact velocities change in the range of 834 mm·s^{-1} and 842 mm·s^{-1}. The velocity derivation does not exceed 10 mm·s^{-1} except at the ball column diameter of 40 mm, which has a velocity derivation of 20 mm·s^{-1}. If only considering the maximum impact velocities with ball column diameter above 50 mm, the change range is 834–842 mm·s^{-1}, which indicates there is little effect of the ball column diameter on the maximum impact velocity of the drill rod. For the maximum rebound velocity, it decreases from 384 mm·s^{-1} to 370 mm·s^{-1} with the increased ball column diameter; however, the reduction rate is 6.3%, which is not significant.

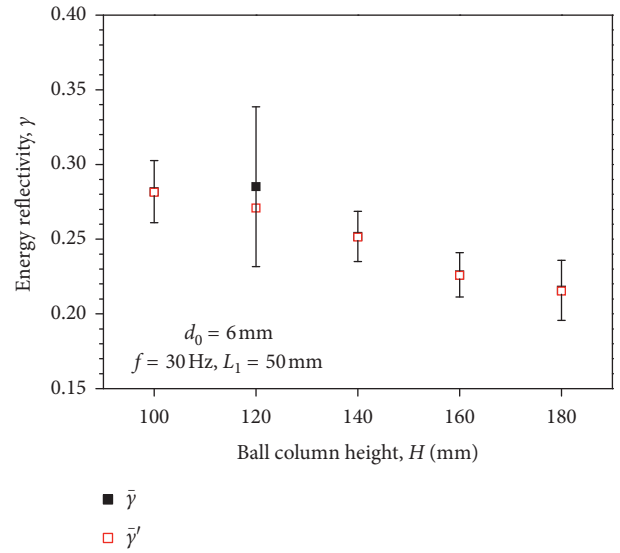

Figure 17: Energy reflectivity under different ball column heights.

Table 5: Filling ratio and porosity of the ball column with different ball column heights.

Compressed column height, H' (mm)	Filled ball number, n	Filling ratio, ϕ	Porosity, λ	Energy reflectivity, γ
90.85	580	0.575	0.425	0.281
107.44	710	0.595	0.405	0.271
126.17	816	0.582	0.418	0.251
142.93	923	0.581	0.419	0.226
163.71	1065	0.585	0.415	0.215

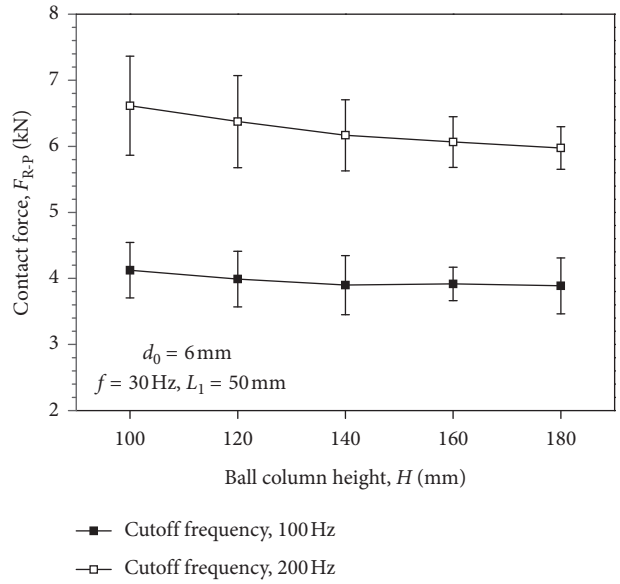

Figure 18: Contact force under different ball column heights.

5.4.2. Energy Reflectivity. There is no difference in the energy reflectivity calculated by the two methods, as shown in Figure 21. The energy reflectivity decreases gradually from 0.223 to 0.196 when the ball column diameter increases from

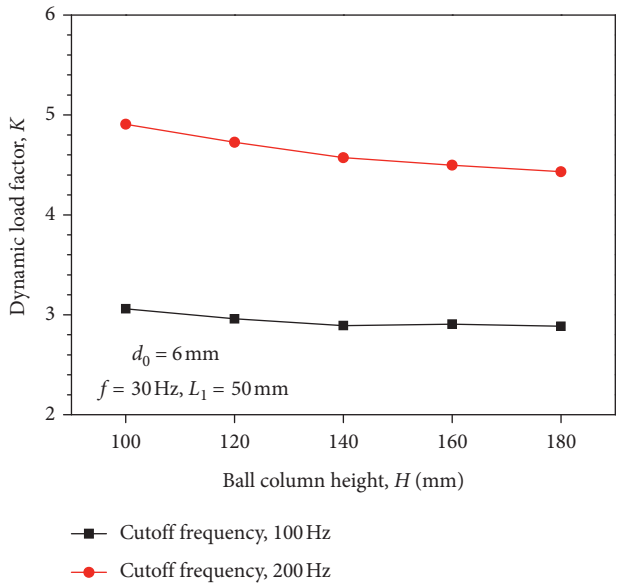

Figure 19: Dynamic load factor under different ball column heights.

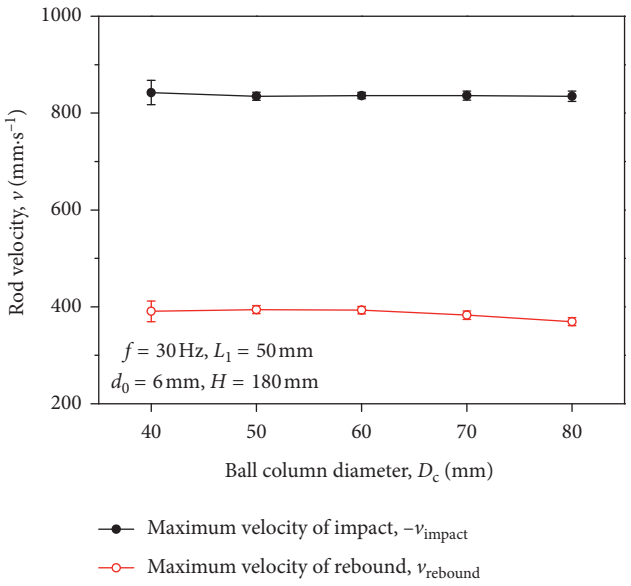

Figure 20: Impact velocity and rebound velocity of the drill with different ball column diameters.

50 mm to 80 mm, and the reduction rate is 12.1%. It seems that an increased ball column diameter will reduce energy reflectivity. By examining the compressed column height and porosity listed in Table 6, it is found that both the compressed column height and porosity increase when the ball column diameter increases from 50 mm to 80 mm. According to the results found, the energy reflectivity is inversely proportional to the compress column height and porosity, so the reduction of energy reflectivity maybe is not caused by the increment of ball column diameter from 50 mm to 80 mm, but the increased column height and porosity.

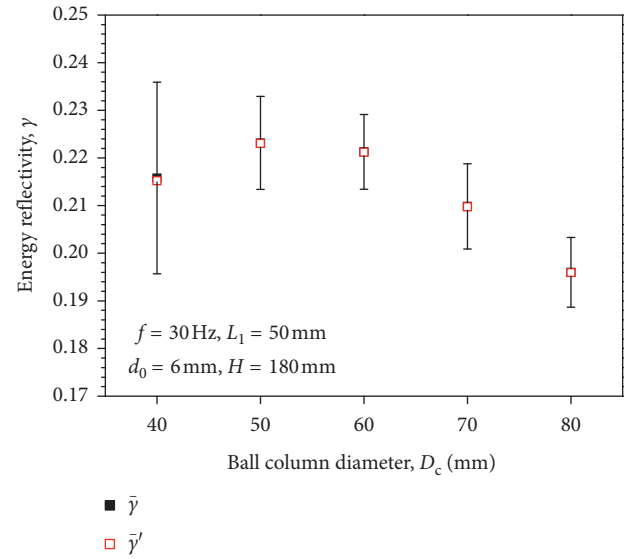

Figure 21: Energy reflectivity under different ball column diameters.

However, it is found that the increased ball column will decrease the energy reflectivity by subtracting the effects of the ball column and porosity as shown in Table 7. The predicted energy reflectivity is obtained by subtracting the effects of the ball column and porosity when the ball column diameter changes. For example, when the ball column diameter changes from 40 mm to 50 mm, the ball column height decreases by 2.55 mm, which will reduce the energy reflectivity by 0.002; the reduction of porosity with 0.049 will reduce the energy reflectivity by 0.013. By eliminating the effects of ball column height and porosity, a predicted energy reflectivity of 0.230 is obtained, which is higher than the actual value of 0.223. A similar result could be found when the ball column diameter changes, so it is regarded that the difference between the predicted value and the actual value is caused by the change of the ball column diameter. The results indicate that the energy reflectivity will reduce with the increase in ball column diameter. Moreover, the smallest energy reflectivity is 0.196 in this group, which is below the allowable value of 0.2 in the standard.

5.4.3. The Contact Force between the Drill Rod and the Piston. The average contact forces and dynamic load factors with different ball column diameters are shown in Figures 22 and 23, respectively. When the ball column increases from 40 mm to 80 mm, the contact force reduces from 3.89 kN to 3.65 kN under the smooth of 100 Hz filter, and the reduction rate is 0.24 kN or 6.1%. However, the contact force changes in the range of 5.97 kN to 6.17 kN under the smooth of 200 Hz filter, and there is no apparent change law. It is regarded that the ball column diameter does not influence the contact force. The same result could be found in Figure 23 that the effect of ball column diameter on dynamic factor is not obvious, with the average values of 2.82 and 4.49 with different filters.

Table 6: Filling ratio and porosity of the ball column with different ball column diameters.

Ball column diameter, D_c (mm)	Filled ball number, n	Compressed column height, H' (mm)	Filling ratio, ϕ	Porosity, λ	Energy reflectivity, γ
40	1065	163.83	0.585	0.415	0.215
50	1776	161.27	0.634	0.366	0.223
60	2664	170.32	0.626	0.374	0.221
70	3597	174.07	0.607	0.393	0.210
80	4773	176.70	0.608	0.392	0.196

Table 7: Predicted energy reflectivity by subtracting the effect of column height and porosity.

Ball column diameter, D_c (mm)	Compressed column height, H' (mm)	Porosity, λ	Effects of H'	Effects of λ	Energy reflectivity, γ	Predicted energy reflectivity, γ
40	163.83	0.415	—	—	0.215	—
50	161.27	0.366	−0.002	−0.013	0.223	0.230
60	170.32	0.374	0.008	0.002	0.221	0.233
70	174.07	0.393	0.003	0.005	0.210	0.229
80	176.70	0.392	0.002	0.000	0.196	0.212

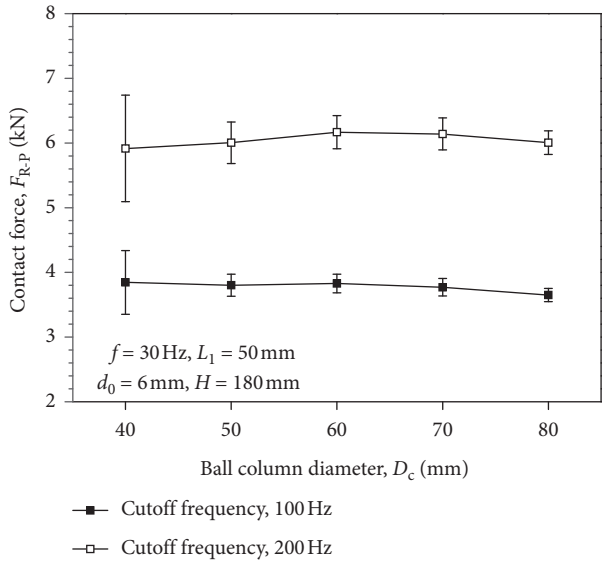

Figure 22: Contact force under different ball column diameters.

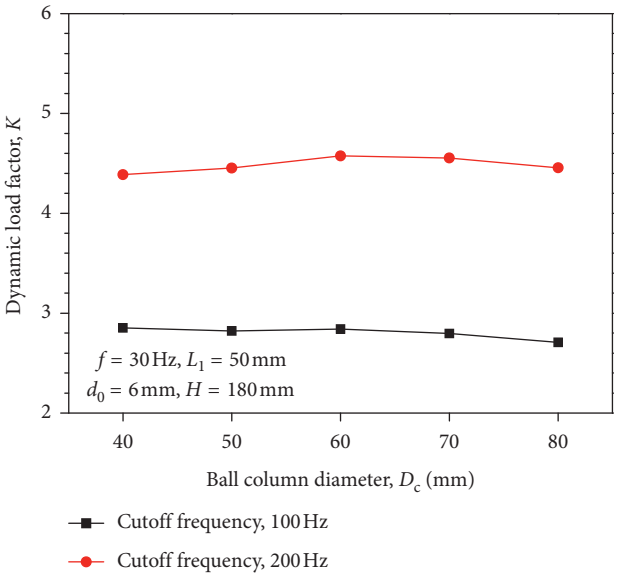

Figure 23: Dynamic load factor under different ball column diameters.

6. Structural Optimization of the Energy Absorber

According to the results in Section 5, the increase in ball column height and diameter will decrease the energy reflectivity. To obtain lower energy reflectivity and verify the influence of ball column height and diameters on the energy absorber, three-parameter combinations with significantly increased ball column height and diameter are designed as (600 mm, 120 mm), (600 mm, 160 mm), and (800 mm, 160 mm). The filling ball diameters are unchanged with 6 mm.

Figure 24 shows the maximum impact velocity and maximum rebound velocity of the drill rod with different ball column height and diameter combinations. When the ball column diameter increases from 120 mm to 160 mm, the maximum impact speed of the drill rod increases slightly. It also brings about an increase in the standard deviation. The increase in the height of the ball column from 600 mm to 800 mm brings a significant reduction in the maximum impact velocity of the drill rod. The rebound speed of the drill rod decreases with the increase in height and diameter of the ball column.

As shown in Figure 25, there is no difference in the energy reflectivity calculated by the two methods. The energy reflectivity decreases from 0.085 to 0.054 when ball column height increases from 120 mm to 160 mm, which meets findings that the increased ball column diameter will decrease the energy reflectivity. With the ball column height increasing from 600 mm to 800 mm, the energy reflectivity decreases from 0.054 to 0.045, and the results are also consistent with the findings that the energy reflectivity is inversely proportional to the ball column height. When the ball column height and diameter combination is (180 mm,

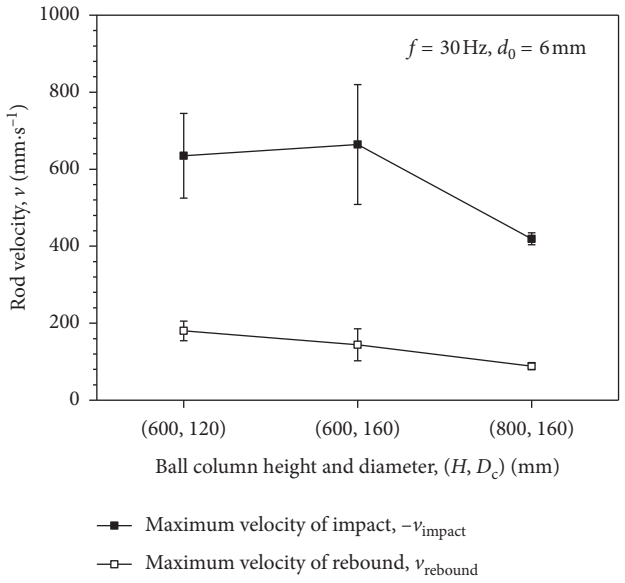

Figure 24: Impact velocity and rebound velocity of the drill with different ball column parameters.

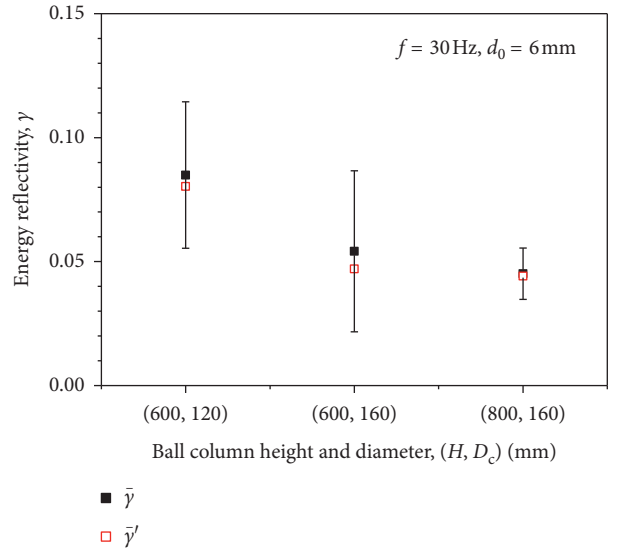

Figure 25: Energy reflectivity with different ball column parameters.

80 mm), the energy reflectivity is 0.196, and it decreases apparently to 0.045 with the parameters of (800 mm, 160 mm).

7. Conclusion

Through numerical simulations, this study presents the working process of a steel ball friction energy absorption structure and evaluated the energy absorption characteristics and the contact force between the drill rod and the piston under different parameters. An equation is proposed to calculate the filling ball numbers in a cylinder with fixed height and diameter, by which the ball number under different stack manner could be calculated. The energy dissipated by the energy absorber is evaluated by the kinetic energy of the drill rod before and after the impact. Within the scope of our numerical research, the following conclusions are obtained:

(1) The energy absorption effect is more evident under higher impact frequency and long impact stroke. The impact frequency and stroke influence the energy absorber by changing the impact force. When the impact frequency and stroke change from (30 Hz, 50 mm) to (40 Hz, 80 mm), which corresponds to the impact force of 1348 N and 3364 N, the energy reflectivity decreases from 0.289 to 0.232.

(2) The filling ball diameter influences the energy reflectivity by changing the porosity, which is negatively correlated to the energy reflectivity. The highest porosity is 0.434, which corresponds to the lowest energy reflectivity of 0.267 with the filling ball diameter equal to 7 mm. However, the energy reflectivity fluctuation is larger, and the filling ball diameter equal to 6 mm with little fluctuation is regarded as the best choice.

(3) The energy reflectivity is inversely proportional to the ball column height. When ball column height increases from 100 mm to 180 mm, the energy reflectivity decreases linearly from 0.281 to 0.215, with a reduction rate of 21%.

(4) By eliminating the effects of ball column height and porosity, the increased ball column diameter will decrease the energy reflectivity that could be found. The energy reflectivity is optimized to 0.196 eventually, which is exactly under the allowable value of 0.2 in the standard, and the corresponding ball column diameter and height are 80 mm and 180 mm, respectively.

(5) Even when the contact force is proportional to the impact frequency and stroke, the dynamic factor decreases by 14% or 12% under different filters. The increase in ball column height will reduce the contact force and the dynamic load factor; the reduction rate is 5.8% or 9.7% under different filters. The changes in ball diameter and ball column diameter have no obvious effect on the contact force and dynamic load factor.

(6) The energy reflectivity is optimized to 0.045 with the ball column diameter and height equal to 160 mm and 600 mm, respectively.

Data Availability

The data used to support the findings of this study were calculated according to the simulation, and they are included in the article. The parameters used in the calculation model were cited from the references listed.

Conflicts of Interest

The author declares that there are no conflicts of interest regarding the publication of this paper.

Acknowledgments

This work was supported by the China Coal Technology & Engineering Group Science and Technology Innovation Fund Project under contract no. 2019-TD-QN019.

References

[1] W. A. Hustrulid and C. Fairhurst, "A theoretical and experimental study of the percussive drilling of rock part I-theory of percussive drilling," *International Journal of Rock Mechanics and Mining Sciences & Geomechanics Abstracts*, vol. 8, no. 4, pp. 311–333, 1971.

[2] W. A. Hustrulid and C. Fairhurst, "A theoretical and experimental study of the percussive drilling of rock part II-force-penetration and specific energy determinations," *International Journal of Rock Mechanics and Mining Sciences & Geomechanics Abstracts*, vol. 8, no. 4, pp. 335–340, 1971.

[3] W. A. Hustrulid and C. Fairhurst, "A theoretical and experimental study of the percussive drilling of rock part III-experimental verification of the mathematical theory," *International Journal of Rock Mechanics and Mining Sciences & Geomechanics Abstracts*, vol. 9, no. 3, pp. 417-418, 1972.

[4] W. A. Hustrulid and C. Fairhurst, "A theoretical and experimental study of the percussive drilling of rock part IV-application of the model to actual percussion drilling," *International Journal of Rock Mechanics and Mining Sciences & Geomechanics Abstracts*, vol. 9, no. 3, pp. 431–442, 1972.

[5] H. Song, H. Shi, Z. Ji et al., "The percussive process and energy transfer efficiency of percussive drilling with consideration of rock damage," *International Journal of Rock Mechanics and Mining Sciences*, vol. 119, pp. 1–12, 2019.

[6] G. Han, M. Bruno, and K. Lao, "Percussion drilling in oil industry: review and rock failure modelling," in *Proceedigs of the AADE 2005 National Technical Conference and Exhibition*, pp. 1–10, Houston, TX, USA, April 2005.

[7] T. Saksala, "3D numerical modelling of bit-rock fracture mechanisms in percussive drilling with a multiple-button bit," *International Journal for Numerical and Analytical Methods in Geomechanics*, vol. 37, no. 3, pp. 309–324, 2013.

[8] T. Saksala, D. Gomon, M. Hokka, and V.-T. Kuokkala, "Numerical and experimental study of percussive drilling with a triple-button bit on Kuru granite," *International Journal of Impact Engineering*, vol. 72, pp. 56–66, 2014.

[9] B. Lundberg and P. Collet, "Optimal wave shape with respect to efficiency in percussive drilling with detachable drill bit," *International Journal of Impact Engineering*, vol. 86, pp. 179–187, 2015.

[10] R. Simon, "Transfer of the stress wave energy in the drill steel of a percussive drill to the rock," *International Journal of Rock Mechanics and Mining Sciences & Geomechanics Abstracts*, vol. 1, no. 3, pp. 397–411, 1964.

[11] L. F. P. Franca, "A bit-rock interaction model for rotary-percussive drilling," *International Journal of Rock Mechanics and Mining Sciences*, vol. 48, no. 5, pp. 827–835, 2011.

[12] B. Lundberg and M. Okrouhlik, "Efficiency of a percussive rock drilling process with consideration of wave energy radiation into the rock," *International Journal of Impact Engineering*, vol. 32, no. 10, pp. 1573–1583, 2006.

[13] B. Lundberg and M. Okrouhlik, "Influence of 3D effects on the efficiency of percussive rock drilling," *International Journal of Impact Engineering*, vol. 25, no. 4, pp. 345–360, 2001.

[14] J. B. Clarke, W. Dalby, and J. F. Gunn, "Chipping hammer vibration," *Scandinavian Journal of Work, Environment & Health*, vol. 12, no. 4, pp. 351–354, 1986.

[15] J. Bitsch, P. Donati, R. Poirot, and L. Roure, "Elaboration of a standard procedure for the measurement of vibration emitted by percussive tools: application to breakers," *Scandinavian Journal of Work, Environment & Health*, vol. 12, no. 4, pp. 347–350, 1986.

[16] International Organization for Standardization (ISO), *Rotary and Percussive Pneumatic Tools - Performance Tests*, International Organization for Standardization, Geneva, Switzerland, 2nd edition, 1984.

[17] International Organization for Standardization (ISO), *Hand-Held Portable Power Tools- Measurement of Vibrations at the Handle-Part 2: Chipping Hammers and Riveting Hammers*, International Organization for Standardization, Geneva, Switzerland, 1992.

[18] J. W. Park and H. E. Kim, "Development of the test system for measuring the impact energy of a hydraulic breaker," in *Proceedings of the 6th JFPS International Symposium on Fluid Power*, Tsukuba, Japan, November 2005.

[19] J. Seo, J.-S. Park, H. Kim, and D. K. Noh, "Experimental evaluation of percussion performance for rock-drill drifter," *Journal of Biosystems Engineering*, vol. 40, no. 1, pp. 1–9, 2015.

[20] J. Seo, D.-K. Noh, G.-H. Lee, and J.-S. Jang, "A percussion performance analysis for rock-drill drifter through simulation modeling and experimental validation," *International Journal of Precision Engineering and Manufacturing*, vol. 17, no. 2, pp. 163–170, 2016.

[21] S. L. Zheng, W. Y. Liu, Y. Y. Mao, X. P. Wang, and J. H. Wang, "Mechanical analysis for the working mechanism of an energy absorber by friction of steel balls," *Mining and Metallurgical Engineering*, vol. 35, no. 4, pp. 21–26, 2015.

[22] R. G. Dong, T. W. McDowell, D. E. Welcome, C. Warren, and A. W. Schopper, "An evaluation of the standardized chipping hammer test specified in ISO 8662-2," *The Annals of Occupational Hygiene*, vol. 48, no. 1, pp. 39–49, 2004.

[23] FunctionBay Inc, *Recurdyn Help V9R3*, FunctionBay Inc, Seongnam, South Korea.

[24] M. C. Marinack, B. G. Gaudio, R. E. Musgrave, C. E. Rizzo, M. Lovell, and C. F. Higgs, "Coefficent of restitution testing: explicit finite element modeling and experiments," in *Proceedings of the STLE/ASME 2010 International Joint Tribology Conference*, pp. 365–367, San Francisco, CA, USA, January 2010.

[25] F. W. Van Name Jr., "Experiment for measuring the coefficient of restitution," *American Journal of Physics*, vol. 26, no. 6, pp. 386–388, 1958.

[26] K. Hashemnia, "Experimental study of the effect of temperature on the coefficient of restitution of steel balls impact to some industrial metal sheets at elevated temperatures," *Powder Technology*, vol. 368, pp. 170–177, 2020.

[27] DEM Solutions Ltd, *EDEM 2020 Documentation*, DEM Solutions Ltd, Edinburgh, UK.